Journal of Applied Remote Sensing

RemoteSensing.SPIEDigitalLibrary.org

Feature-constrained registration of building point clouds acquired by terrestrial and airborne laser scanners

Hangbin Wu
Marco Scaioni
Hanyan Li
Nan Li
Minfeng Lu
Chun Liu

SPIE.

Feature-constrained registration of building point clouds acquired by terrestrial and airborne laser scanners

Hangbin Wu,[a,*] Marco Scaioni,[a] Hanyan Li,[b] Nan Li,[a] Minfeng Lu,[a] and Chun Liu[a]

[a]Tongji University, College of Surveying and Geo-infomatics, Siping Road 1239, Shanghai 200092, China

[b]Georgia Institute of Technology, Department of Civil and Environmental Engineering, Atlanta, Georgia 30332

Abstract. Point-cloud registration is usually accomplished on the basis of several corresponding features to compute the parameters of the transformation model. However, common point features are difficult to select because airborne laser scanner (ALS) and terrestrial laser scanner (TLS) point clouds of the same object have be aligned due to the different sensing positions and sampling modes. Taking building profile features as objects, a registration method based on feature constraints is proposed here. The standard six-parameter rigid-body transformation adopted for alignment of laser scans is replaced by a two-step transformation: horizontal registration based on a two-dimensional similarity transformation and vertical registration based on a simple vertical shift. First, the feature-line and feature-plane equation parameters are obtained from both the airborne and terrestrial point clouds. Second, the plane transformation parameters are computed after projecting the extracted features onto a horizontal reference plane. Finally, the elevation transformation parameter is calculated by comparing the heights of flat features. The ALS and TLS datasets of two buildings (Shanghai Pudong International Conference Center and Shanghai Ocean Aquarium, China) were used to evaluate the robustness and accuracy. The results show that the proposed feature-constrained method works well for registration between two datasets. Five checkpoints and one overlap zone for the Pudong International Conference Center were selected to evaluate the accuracy and resulted in accuracies of 0.15 to 0.5 m in the horizontal direction and 0.20 m in the vertical direction. [DOI: 10.1117/1.JRS.8.083587]

Keywords: laser scanning; feature extraction; registration; coordinate transformation; point cloud.

Paper 14140 received Mar. 10, 2014; revised manuscript received May 13, 2014; accepted for publication Jun. 5, 2014; published online Jul. 18, 2014.

1 Introduction

After more than two decades of development, both airborne laser scanning (ALS) and terrestrial laser scanning (TLS) technologies have become highly operational in their respective domains for surface reconstruction and information extraction.[1–3] Both of these technologies measure the distance between the objects and a laser sensor. The knowledge of the attitude angles of the laser rangefinder integrated with information on the absolute position of the sensor (from Inertial Measurement Unit, Global Navigation Satellite System, or ground control points) is used to determine the three-dimensional (3-D) coordinates of the mass points, referred to as a point cloud. The observation point-of-view of ALS and TLS is quite different due to the placement of the sensors, and the same object scanned by different platforms will produce complementary data. Indeed, TLS may scan a point cloud depicting different sides of the building from a set of ground-based standpoints, while the 3-D information on the building roof can be acquired by

*Address all correspondence to: Hangbin Wu, E-mail: hb@tongji.edu.cn

0091-3286/2014/$25.00

ALS.[4] A complete building model could most likely be established from the fusion of the two datasets after their registration into the same reference system.

The problem addressed in the field of laser scanning can be extended directly to the case of point clouds derived from image-based methods such as photogrammetry and computer vision.[5] Indeed, it has been demonstrated that these techniques might provide dense surfaces that feature spatial resolution and precision on 3-D coordinates similar to the values obtainable from laser scanning.[6] Additionally, the possibility of registering image-based point clouds and laser scans has recently been discussed in the literature.[7]

A common approach for point-cloud registration is to use artificial targets as the source and target references. The targets are typically objects (for example, small spheres) that are invariant with respect to the scanner viewpoint.[8] Usually, they are composed of retro-reflective material to simplify their automatic recognition.[9] Many commercial software packages support automatic registration with such targets, including automatic target recognition and estimating the registration transformation with the targets as reference points. Typically, a 3-D rigid-body transformation (three shifts and three rotations in space) is implemented, with the scale known because of the direct measurement of ranges. In Ref. 10, some considerations for estimating this type of model are discussed, particularly regarding the reliability of the observation and the spatial distribution of points.

To avoid deploying targets at the scene, considerable research on the automatic registration of point clouds has been carried out. The existing algorithms can be divided into two main groups: (1) point-based and (2) feature-based methods. In the former, the iteratively closest point (ICP) algorithm together with its improvements is the most popular method for aligning two point clouds.[11,12] This algorithm begins with two point clouds referred to different reference systems that must first be approximately prealigned by the manual measurement of some correspondences or another automatic technique that can provide a rough registration. The concept is the iterative refinement of the rigid-body transformation by alternating the steps of identifying corresponding points across the two point clouds and determining the best rotation and translation parameters to minimize an error metric based on the distance between corresponding points. There are many variants and extensions of the initial algorithm designed to increase computational efficiency, robustness, or convergence. As the ICP, the matching step is the most time-consuming part of the registration phase, and the integration of the ICP algorithm with random sample consensus (RANSAC) or least the median of squares (LMS) estimators were proposed by Ref. 13 to improve the efficiency and robustness.

Reference 14 presented an algorithm that significantly reduces the level of registration errors between all pairs in a set of range views. Erroneous associations between nearest points might frequently occur in scans acquired with different point densities or from different points-of-view,[15] such as when ALS and TLS data are merged. For these reasons, ICP is often utilized to compute the registration between two partially overlapping point clouds that were both scanned by the same type of platform, but it is rarely applied to align different data categories.

Corner points of buildings are typical types of feature points in urban areas. References 16 and 17 proposed a semiautomatic method for coregistration of ALS and TLS point clouds. The corner points of buildings are first separately extracted from both datasets. Then a manual selection is performed to hire the corner points as corresponding feature pairs. Then the feature pairs are introduced into a similarity transformation model to obtain translations, rotations, and the scale parameter between the coordinate systems.

Feature-based methods consist of the extraction of corresponding feature primitives such as key points (such as the ones computed by the scale-invariant feature transform or speeded up robust features operators),[18,19] planes,[20] and surfaces.[21] References 22 and 23 demonstrated the possibility of applying standard interest operators and feature-based matching (FBM) techniques used for image registration to align laser point clouds. First, the intensity images for each scan are aligned using FBM techniques. Then, the final rigid-body transformation is computed using the corresponding 3-D coordinates on the laser scans. Reference 24 used a scale-space representation to detect a set of salient feature points. For each feature point, a significance vector is computed that is treated as an approximately invariant under rigid transformations. The extracted signed feature set is used to obtain an approximate alignment of the two surfaces. Similarly, Refs. 25 and 26 extended the method to the contemporary registration of several scans. As

lines or planes extracted from a point cloud are fitted by estimation on the basis of many points, using such 3-D signatures as registration features is expected to offer better results than using feature points. Reference 27 proposed an autonomous matching procedure based on planar patches that were automatically estimated by a region growing algorithm. Following their extraction, patches from different scans are matched subject to certain geometric constraints. The extraction of the planar patches requires the segmentation of different scans, a task that might become quite complex in cluttered scenes. Reference 28 used a variation in curvature as the matching criterion on local points, which required the computation of the normal vector and the curvature.[29] Reference 30 proposed a method using the 3-D line features derived from both terrestrial and airborne point clouds for a two-steps (coarse and fine) registration. Unfortunately, these measures are prone to being affected by noise because of the dependency on the second-order derivatives, which is the main shortcoming of feature-based techniques.

The drawbacks of both categories of registration methods become even more critical when airborne and terrestrial point clouds are to be registered together. Indeed, the different points-of-view and the sparse point cloud on the vertical surfaces (such as building façades) which are poorly sampled from airborne sensors make the registration process highly complex.

For the sake of completeness, the coregistration of ALS and TLS data could also be carried out using direct-geo-referencing techniques. Indeed, ALS data are geo-referenced using this approach, which is strictly required for the determination of 3-D coordinates when the sensor is moving. Static TLS data can also be geo-referenced in this way, as proposed by Refs. 31 and 32. However, this method requires successive refinements to cope with possible bias between the adopted reference systems.

To overcome the limitations of existing techniques in such applications, this paper proposes a registration method based on building-boundary extraction from both ALS and TLS laser data. Unlike the standard consolidated practice in laser scanning data processing, 3-D registration uses the simplified 3-D similarity transformation (or Bursa) model instead of rigid-body transformation. Based on building features from different datasets, the paper establishes a constrained relationship between the building parameters and the transformation model parameters. Planar and elevation/transformation parameters are then computed using the least squares (LS) method with redundant observations. In Sec. 5, the method is evaluated using two datasets consisting of ALS and TLS data for two buildings (Pudong International Conference Center and Shanghai Ocean Aquarium) in the Pudong district, Shanghai, China. Finally, in Sec. 6, conclusions are described.

2 Principle of Point-Cloud Registration

2.1 *Problem Definition*

To clearly describe the two different reference systems adopted for the ALS and TLS datasets, ARS $(X_A Y_A Z_A)$ is defined as the airborne reference system and TRS $(X_T Y_T Z_T)$ is defined as the terrestrial reference system. The ARS is regarded as the target system, while the TRS is treated as the source system. The problem of point-cloud registration is to find a suitable registration model and calculate the model parameters to map the source onto the target reference. In this section, the mathematical model for the registration and the principle of the calculation method are described.

2.2 *Selection of the Registration Model*

The essence of the registration method between ALS and TLS data is the adopted transformation model. Indeed, 3-D coordinate transformations are usually assumed to define the geometric relationship between two spatial reference systems on the basis of global parameters such as an isotropic scale, a 3-D shift vector, and a spatial rotation matrix. Therefore, the model plays a paramount role in this type of problem and directly affects the final accuracy of the registered coordinates. Usually, the scale is not estimated when two laser scanning datasets are registered, as already noted in the end of Sec. 1. Indeed, laser scanning can directly measure distances that define the scale, unlike photogrammetry which is actually based on the measurement of directions.

The 3-D similarity transformation is the usual model for generic coordinate transformations. It is also normally referred to as the 3-D conformal transformation or Bursa model. In this model, the source reference $(o-xyz)$ could be transformed into the target reference system $(O\text{-}XYZ)$ according to the following equation:

$$\begin{bmatrix} X \\ Y \\ Z \end{bmatrix} = \mu R(\alpha,\beta,\gamma)\begin{pmatrix} x \\ y \\ z \end{pmatrix} + \begin{pmatrix} \Delta x \\ \Delta y \\ \Delta z \end{pmatrix}, \tag{1}$$

where μ is the scale factor; α, β, and γ are the rotations around the Z-axis, Y-axis, and X-axis, respectively, which parameterize the rotation matrix R; and Δx, Δy, Δz are the components of the 3-D translation vector.

Point clouds obtained from the ALS system are usually based on a local datum or on a mapping coordinate system. The Z-axis of $X_A Y_A Z_A$ is approximately aligned along the local plumb line. Meanwhile, the TLS instrument is leveled by a level plummet[33,34] or by using the internal leveling automatic system when scanning the terrain objects. Therefore, the Z-axis of $X_T Y_T Z_T$ is approximately aligned to the Z-axis of $X_A Y_A Z_A$. Therefore, the horizontal rotation angles (β and γ) in the rotation matrix R can be regarded as zero. Consequently, the similarity transformation model could be simplified to only three shift parameters $(\Delta x, \Delta y, \Delta z)$, one rotation angle (α) around with Z-axis, and the scale parameter (μ):

$$\begin{pmatrix} X_A \\ Y_A \\ Z_A \end{pmatrix} = \begin{bmatrix} \mu\cos\alpha & \mu\sin\alpha & 0 \\ -\mu\sin\alpha & \mu\cos\alpha & 0 \\ 0 & 0 & \mu \end{bmatrix}\begin{pmatrix} X_T \\ Y_T \\ Z_T \end{pmatrix} + \begin{bmatrix} \Delta x \\ \Delta y \\ \Delta z \end{bmatrix}. \tag{2}$$

In many geodetic applications, Eq. (2) is solved through a two-step procedure. In the first stage, by using common points in the source and target reference systems, the model parameters are computed using LS or robust estimators to cope with outliers [e.g., RANSAC, and LMS.[35]] Then, in a second stage, the estimated parameters are assumed to be known, and the coordinates of the noncommon points in the source system are mapped into the target system. However, as above, common points between the ARS and TRS are difficult to find. Both linear features extracted from ALS data and polygonal features from the TLS data are used to provide correspondences for estimating the unknown parameters in Eq. (2).

2.3 *Principle of Feature-Constrained Registration Between ALS and TLS Data*

Terrestrial and airborne light detection and ranging (LiDAR) systems are different platforms that can be used to capture point clouds from different points of view. In Fig. 1, black dots denote the

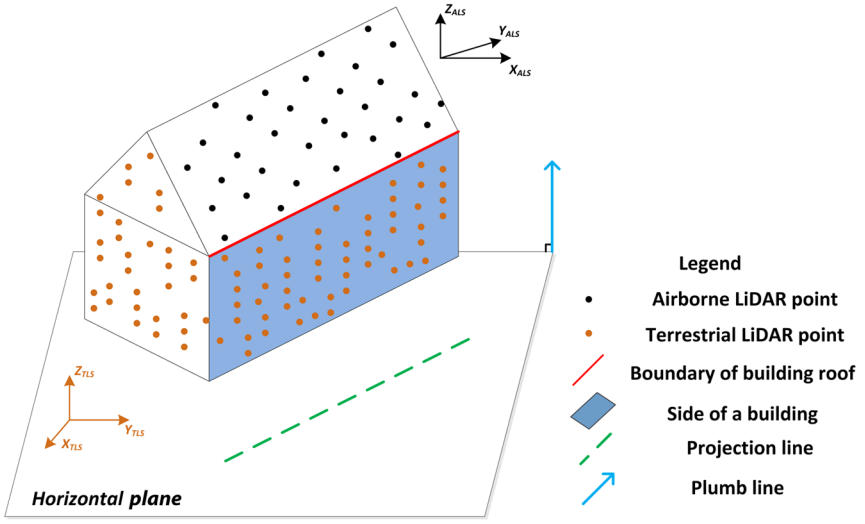

Fig. 1 The principle of data registration using building features.

ALS 3-D points while red dots denote the TLS point cloud. The red line represents the boundary contour of the building roof and the blue polygon denotes one of the façades of the building. The roof boundary contour and the façade surface could be easily extracted from ALS and TLS data, respectively, as introduced in Sec. 3. In the real scene, the red line feature is a part of the façade polygon. Both of them can be perpendicularly projected into the same line on a horizontal plane adopted as a reference (the green dashed line in Fig. 1). Therefore, these features are exploited as constraints between the ARS and TRS to estimate the registration parameters. The detailed steps of this procedure will be described in Sec. 4.

2.4 *Flowchart of the Proposed Method*

The flowchart of the proposed method is integrated with three main steps (Fig. 2), namely, (1) feature extraction and feature parameter computation; (2) horizontal model parameter computation; and (3) vertical model parameter computation. The segmentation of point clouds, both terrestrial and airborne, is first used to obtain the different parts of the whole building dataset. Then, the feature extraction methods and feature parameter computations are applied to the different subdatasets of the building. The horizontal model parameter is computed according to the procedure described in Sec. 4.1. Eventually, the vertical shift parameter is calculated as described in detail in Sec. 4.2. The estimated model parameters can be evaluated for accuracy during the second and third steps using independent checkpoints.

Due to the vertical setup of the Z-axis in both reference systems adopted for the ALS and TLS data, the registration process can be separated into two steps. First, the horizontal transformation parameters can be computed using a method based on the extracted linear features and constraints. Next, four of the total five parameters ($\Xi_h = [\alpha \quad \Delta x \quad \Delta y \quad \mu]^T$) of the simplified similarity Eq. (2) can be computed.

Second, to accurately compute the unique remaining unknown parameter ($\Xi_v = [\Delta z]^T$), a fitting procedure is applied to the small overlap area between the roof points, as captured by both laser scanning systems. The details of these steps will be introduced in the following sections.

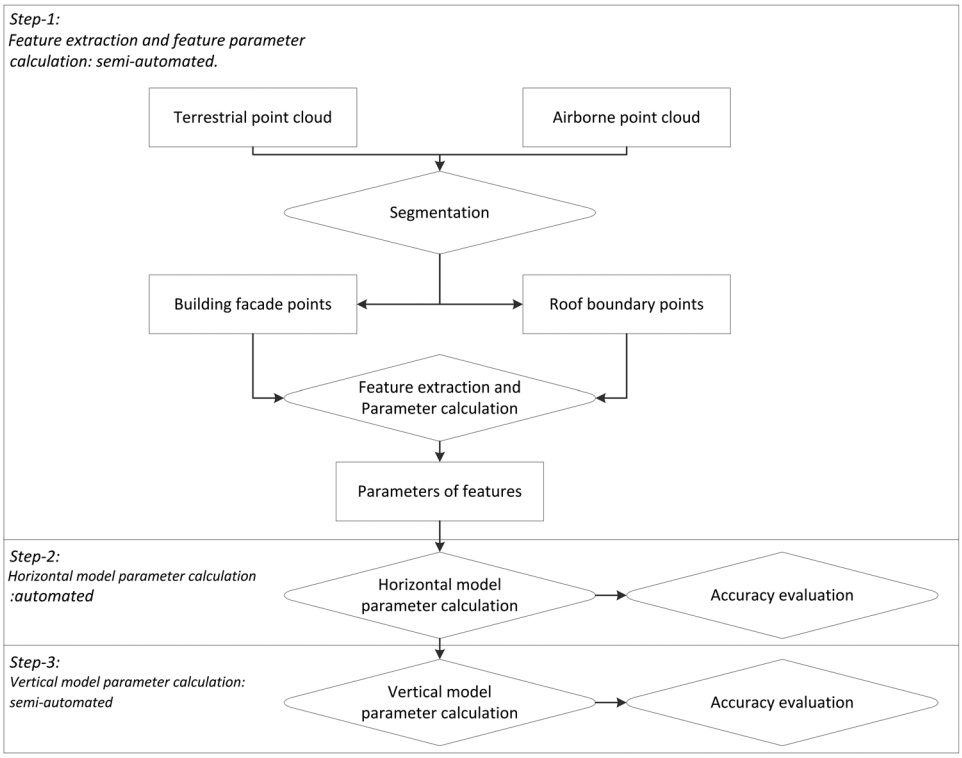

Fig. 2 Flowchart of the method adopted for registration of airborne and terrestrial point clouds.

3 Independent Feature Extraction from Laser Scanning Datasets

3.1 *Roof Boundary Line Extraction and Parameter Adjustment from ALS Point Cloud*

The extraction of the roof contour line and the computation of its parameters are described in this section. Although automatic building methods outlining the extraction methods have been published, e.g., Ref. 36 in this paper, the semiautomatic operations are used to obtain the boundary line of the building. As a preliminary operation, the portion of the whole airborne point cloud that contains the target building must be extracted using classification methods by Terrasolid, which was developed by a Finnish company. The parameter computing procedure is based on two steps. First, the point cloud of the building in the target system $(X_A Y_A Z_A)$ is used to classify the edge points, and the initial feature parameters are computed using a model-fitting procedure. Then, the estimated parameters of the roof boundary features are refined in a second step.

The roof boundary contour line of the building in the ALS dataset is a 3-D line. From this feature, a two-dimensional (2-D) line must be derived in the horizontal plane to be used for registration, as shown by the green dashed line in Fig. 1. As the point cloud was collected using a local coordinate system and local geoid, the ALS point cloud is projected into the horizontal plane (see Fig. 3) with the Z vector as zero. The boundary points are then extracted by the Canny operator.[37] The boundary points usually consist of interior points which must be segmented into simple lines. In this paper, the complete contour was manually segmented into single elements.

Using the boundary points, a linear model is fitted to obtain the line parameters (K_i, B_i) of each line feature i together with the fitting accuracy $\hat{\sigma}_{0Ai}$ and the covariance matrix Q_{AAi} of the estimated parameters. Here, K_i denotes the slope parameter for a 2-D line and B_i denotes the intercept. Each segment of the fitting boundary could be presented as

$$Y = K_i X + B_i. \tag{3}$$

The boundary points used for fitting lines could not represent the precise boundary of a building roof because of the noise of the reflectance of material and the discrete sampling by the ALS system. Most of the boundary points are located near or on the boundary, but not at extract boundary (see Fig. 4). Therefore, the fitted boundary line differs from the real position of the roof edge. Here, a parallel shift adjustment is used to improve the accuracy of the fitted boundary. Under the hypothesis that the outmost point is located at the boundary, the shift d in Fig. 4 is the distance between the outmost point and the fitted boundary.

The fitted boundary will split all points into two groups: the outer points (see blue dots in Fig. 3) and the inner points (yellow dots). The outer points are located between the fitted

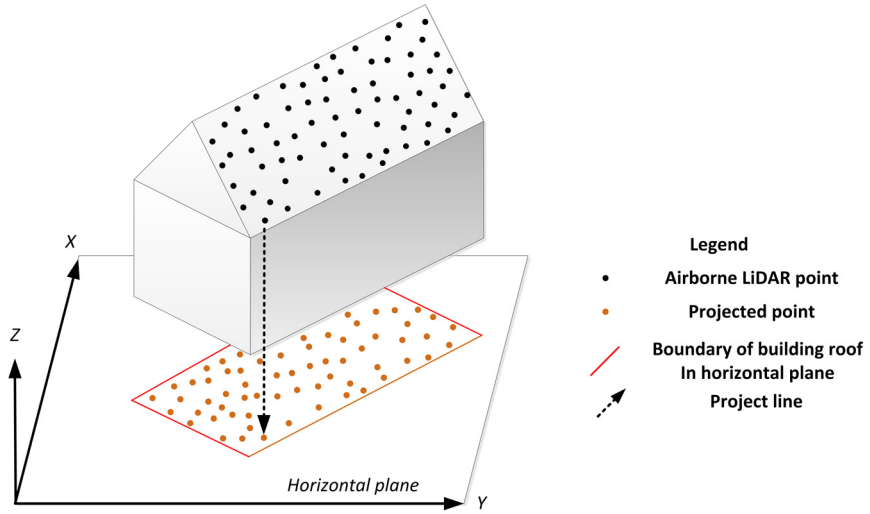

Fig. 3 Schematic diagram of the projection of the airborne laser scanner (ALS) point cloud onto the horizontal plane.

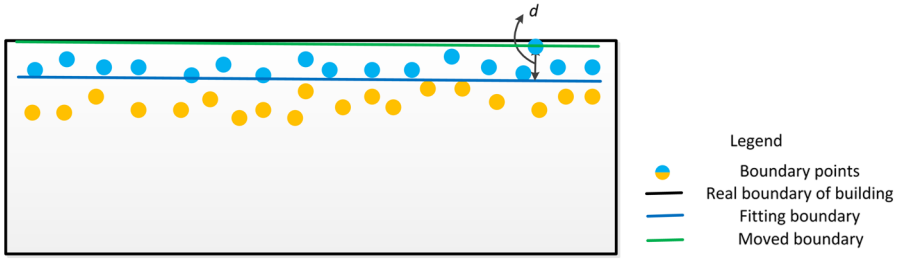

Fig. 4 Line feature extraction and adjustment from airborne boundary points in a horizontal view.

boundary and the real boundary while the inner points are located on the opposite side. The outmost point is one of the outer points which is located furthest away from the fitted boundary.

After the parallel shift, the relocated boundary is regarded as the best-fit boundary to represent the real contour of the building roof that will be used for registration in Sec. 4. However, to avoid error when the outmost point is an outlier, a manual check is also performed before each feature is shifted.

With reference to Fig. 5, let LA be the boundary line fitting the boundary points and d be the distance from the outmost point to LA (index i that identifies the i'th bounding feature will be omitted hereafter). After a shift d in the direction orthogonal to the extracted boundary LA, the output boundary feature will be termed as LB. According to the relationship between the boundary features LA and LB, the parameters describing the new line (i.e., K_{LB} and B_{LB}) can be computed by

$$B_{\mathrm{LB}} = B_{\mathrm{LA}} + \Delta b = B_1 + \frac{d}{\cos\,\varphi} \tag{4}$$

$$K_{\mathrm{LB}} = K_1 = \tan\,\varphi, \tag{5}$$

where φ is the angle between LA and the X-axis. B_{LB} and B_{LA} are the intercept parameters of lines LB and LA, while B_1 and K_1 are the intercept and the slope parameter of line 1. K_{LB} is the slope parameter of line LB.

3.2 *Roof Boundary Line Extraction From TLS Point Cloud*

The terrestrial point cloud of a building usually describes the external façades. Several papers have been published in order to obtain the façade points from a point cloud.[38,39] Therefore, it is easy to obtain each single 3-D plane (the blue polygon in Fig. 1) using a model fitting approach for the segmentation of the whole point cloud.[40] To derive the best-fitting plane, an iterative procedure is used for the LS estimate of the parameters (P_1, P_2, and P_3) according to the equation

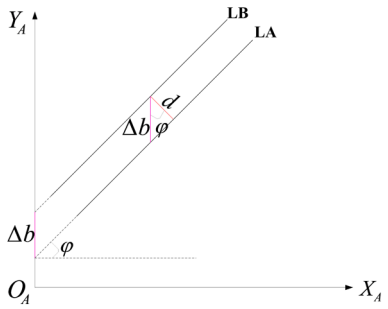

Fig. 5 Improvement of the extraction of single building boundary feature parameters from ALS dataset, after projection onto the horizontal plane.

$$P_1X + P_2Y + P_3Z = 1. \tag{6}$$

After any iteration, the points featuring larger absolute residuals [usually three times the root-mean-square error (RMSE)] will be removed, and the LS solution will be recomputed. This procedure is intended to reduce the number of noisy points.

To establish the relationship between the same features captured in the ALS and TLS point clouds, the 3-D plane function will also be projected onto a 2-D line in the horizontal plane (green dashed line in Fig. 1). In this plane, the model in Eq. (6) is simplified as follows because of the constant elevation Z

$$P_1X + P_2Y = 1. \tag{7}$$

Then, the above function is converted into the slope-intercept model to make it comparable with the parameters estimated from the ALS data

$$y = kx + b, \tag{8}$$

where

$$k = -\frac{P_1}{P_2}, \qquad b = \frac{1}{P_2}. \tag{9}$$

4 Point-Cloud Registration Using Common Features of Building

4.1 *Horizontal Model Parameter Estimates*

The horizontal parameters Ξ_h of the simplified similarity model are estimated using the two sets of linear features extracted from the ALS and TLS datasets. As shown in Fig. 6, LT is the projected boundary feature extracted from the TLS point cloud and LA is the boundary feature of the corresponding façade extracted from the ALS point cloud. In this paper, we manually ensure the relationship between LT and LA with the assistance of digital maps or pictures of scanned object. This will reduce the possibility of mismatching.

Suppose we have a pair of generic points with index i and j in LT, whose coordinates are (X_T^i, Y_T^i) and (X_T^j, Y_T^j), respectively, and their corresponding two points (index I and J) in LA, with coordinates (X_A^I, Y_A^I) and (X_A^J, Y_A^J), respectively. For any pair of points in the horizontal plane, one can define the corresponding line function.

The parameters of line LT (K_T^{ij}, B_T^{ij}) and line LA (K_A^{IJ}, B_A^{IJ}), whose estimates have already been described in Secs. 3.1 and 3.2, are used below. According to the model parameters in vector Ξ_h, which expresses the horizontal component of the transformation between the TLS and ALS point clouds, the coordinates of both points can be calculated from the following equations:

$$\begin{cases} X_A^I = \mu X_T^i \cos\alpha + \mu Y_T^i \sin\alpha + \Delta x \\ Y_A^I = -\mu X_T^i \sin\alpha + \mu Y_T^i \cos\alpha + \Delta y \end{cases} \tag{10}$$

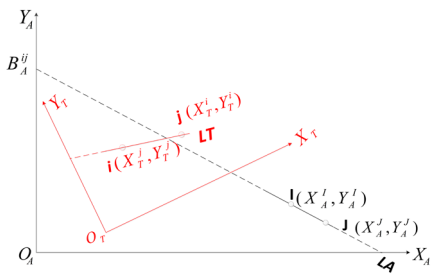

Fig. 6 The linear features in the terrestrial reference system and airborne reference system after projection onto the horizontal plane.

$$\begin{cases} X_{\mathrm{A}}^{J} = \mu X_{\mathrm{T}}^{j} \cos\alpha + \mu Y_{\mathrm{T}}^{j} \sin\alpha + \Delta x \\ Y_{\mathrm{A}}^{J} = -\mu X_{\mathrm{T}}^{j} \sin\alpha + \mu Y_{\mathrm{T}}^{j} \cos\alpha + \Delta y \end{cases}. \tag{11}$$

Then, the slope parameters can be calculated as follows:

$$K_{\mathrm{A}}^{IJ} = \frac{Y_{\mathrm{A}}^{J} - Y_{\mathrm{A}}^{I}}{X_{\mathrm{A}}^{J} - X_{\mathrm{A}}^{I}}. \tag{12}$$

By substituting Eqs. (10) and (11) into Eq. (12), the slope parameter of the LA could be derived as follows:

$$K_{\mathrm{A}}^{IJ} = \frac{-(X_{\mathrm{T}}^{j} - X_{\mathrm{T}}^{i})\sin\alpha + (Y_{\mathrm{T}}^{j} - Y_{\mathrm{T}}^{i})\cos\alpha}{(X_{\mathrm{T}}^{j} - X_{\mathrm{T}}^{i})\cos\alpha + (Y_{\mathrm{T}}^{j} - Y_{\mathrm{T}}^{i})\sin\alpha}. \tag{13}$$

In the TLS system, points i and j are located in LT. Therefore, the coordinates of points i and j should satisfy the following equation:

$$\begin{cases} Y_{\mathrm{T}}^{i} = K_{\mathrm{T}}^{ij} X_{\mathrm{T}}^{i} + B_{\mathrm{T}}^{ij} \\ Y_{\mathrm{T}}^{j} = K_{\mathrm{T}}^{ij} X_{\mathrm{T}}^{j} + B_{\mathrm{T}}^{ij} \end{cases}. \tag{14}$$

The slope parameter can ultimately be obtained by substituting Eq. (14) into Eq. (13)

$$K_{\mathrm{A}}^{IJ} = \frac{-\tan\alpha + K_{\mathrm{T}}^{ij}}{1 + K_{\mathrm{T}}^{ij}\tan\alpha}. \tag{15}$$

Equation (15) describes the relationship between the rotation α in the simplified similarity transformation model and the feature parameters K_{T}^{ij} and K_{A}^{IJ} as computed from the segmented data. Using a similar transformation process, the intercept parameter of LA could be described using the following equation:

$$B_{\mathrm{A}}^{IJ} = \frac{\mu B_{\mathrm{T}}^{ij} + \Delta y(\cos\alpha + K_{\mathrm{T}}^{ij}\sin\alpha) + \Delta x(\sin\alpha - K_{\mathrm{T}}^{ij}\cos\alpha)}{\cos\alpha + K_{\mathrm{T}}^{ij}\sin\alpha}. \tag{16}$$

By combining Eqs. (15) and (16), the constraint relationship between the feature parameters (slope and intercept of the line) and the model parameter vector Ξ_{h} can be established. The features extracted in Sec. 3 should theoretically satisfy Eqs. (15) and (16). Therefore, four parameters could be calculated using one set of slope parameters (K_{T}^{ij} and K_{A}^{IJ}) and three sets of intercept parameters (B_{T}^{ij} and B_{A}^{IJ}). When redundant observations exist, e.g., in the case that three sets of features were extracted, the model parameters could be obtained using the LS estimate. In this case, Eqs. (15) and (16) should be linearized (see Appendix A).

4.2 *Vertical Model Parameter Estimates*

The vertical parameter Ξ_{v} of Eq. (2) could not be computed using the same method illustrated for the horizontal component Ξ_{h}. The vertical parameter mainly describes the shift ΔZ between the target and source systems. Therefore, a different procedure is implemented here, consisting of three steps. The first step is to fit a flat roof edge to all the roof edge points. After filtering those points with residuals featuring the highest RMSE, the average elevation of the roof edge ($\bar{Z}_A$) in the ALS dataset can be obtained

$$\bar{Z}_A = \frac{1}{n}\sum_{i=1}^{n} Z_A^i, \tag{17}$$

where n denotes the number of valid points with elevation Z_A^i used in the averaging process.

Then, the TLS data were used to slice the points at the top of the building as the second step. The whole TLS point cloud can be segmented into different vertical layers by the

depth interval. Then, the average elevation of the building roof ($\bar{Z}_T$) was computed from the points of the top layer

$$\bar{Z}_T = \frac{1}{m}\sum_{i=1}^{m} Z_T^i, \tag{18}$$

where m denotes the number of points on the top layer.

At the third step, ΔZ was computed by the following equation, according to Eq. (2)

$$\Delta z = \bar{Z}_A - \mu \bar{Z}_T. \tag{19}$$

5 Case Studies

In this section, two experiments concerning the data registration between the ALS and TLS point clouds of two buildings are presented and discussed. The reference system of the ALS point cloud is considered as the target system, while the reference system of the TLS point cloud is taken as the source system. The following sections include the description of the two datasets, the feature extraction stage, the estimate of the simplified similarity Eq. (2), and the evaluation of the achieved accuracy.

5.1 *Case Study Buildings and Datasets*

Two buildings in the Pudong district, Shanghai, China, were used as case studies. The first building is the Pudong International Conference Center (Pudong ICC) and the second is the Shanghai Ocean Aquarium.

The size of the Pudong ICC building is approximately 160 m × 100 m × 60 m (length × width × height). The ALS point cloud was captured in 2006 using an ALTM 3100 LiDAR system (Optech Company, Toronto, Canada), providing 76,426 points for the case study building. The adopted reference system is the local mapping system established by the Shanghai Municipality. The average point spacing is 0.16 m. The ALS point cloud is shown in Fig. 7(a).

The TLS point cloud was captured using a focus 3-D phase-shift laser scanner (http://www.faro.com/en-us/products/3d-surveying/faro-focus3d/overview) on March 2013. During the data acquisition, 21 stations were set up at an average distance of 30 m apart. The point cloud captured from each station was referenced to the topocentric vertical system of each station, whose vertical axis had been aligned along the local plumb line using a bubble-level sensor. After preprocessing, including cutting and compressing, all laser scans were registered together using the ICP method. The output point clouds were referenced to a project topocentric reference system (the intrinsic reference system of the first station was assumed to establish the TLS datum) and consisted of a total of 635,941 points with an average point spacing of 0.12 m. The TLS point cloud is shown in Fig. 7(b).

A second case study is the Shanghai Ocean Aquarium, which includes two adjacent buildings. The sizes of the two buildings are 65 m × 65 m × 40 m and 48 m × 37 m × 20 m. As in the Pudong ICC, the ALS point cloud and TLS point cloud were scanned using ALTM and FARO Focus 3-D.

The ALS point cloud was captured in 2006 and consists of 37,901 points. The average point spacing is approximately 0.16 m. The TLS point clouds were obtained at the end of December 2013. During the data acquisition, 14 stations were set up at a minimum distance of 20 m apart. Taking the first reference system (RS) as the RS, after preprocessing the output point cloud contains 381,658 points. The average point spacing of the TLS point cloud is 0.11 m. The datasets are shown in Fig. 8.

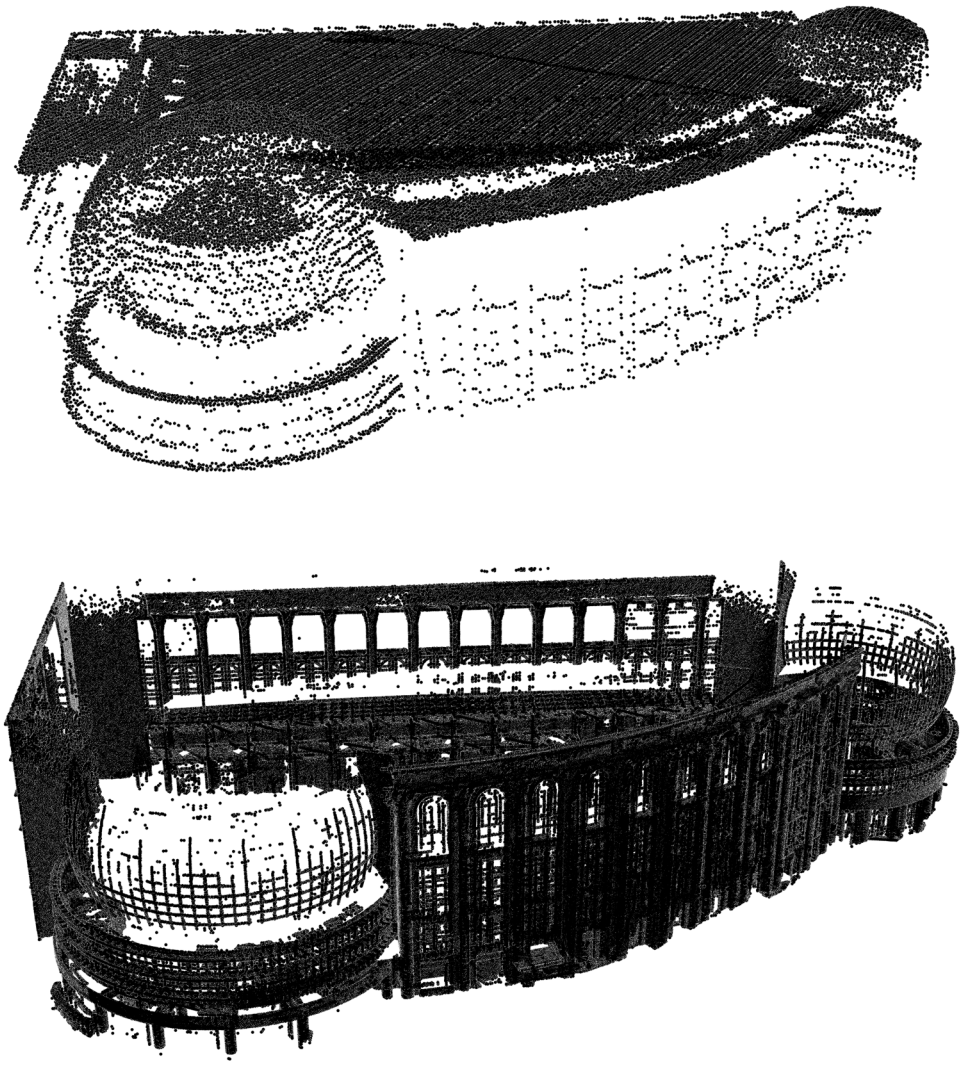

Fig. 7 The first building used to assess the registration method (Pudong International Conference Center—Pudong ICC): (a) ALS point cloud and (b) TLS point cloud.

5.2 *Feature Extraction from ALS and TLS Datasets*

5.2.1 *Feature parameters extracted for the Pudong ICC building*

The south and east façades of the Pudong ICC building consist of simple linear and polygonal features (see Fig. 9). Consequently, the features can be easily extracted from both the TLS and ALS point clouds using the methods introduced in Sec. 3.

In this experiment, four linear features (red lines in Fig. 9) were selected to apply the registration procedure. The feature lines were manually selected from the two datasets to make sure the correspondence between the ALS and TLS features was correct. Table 1 shows the computed slope and intercept parameters of the linear features in the horizontal planes of the corresponding systems.

5.2.2 *Feature parameters extracted for Shanghai Ocean Aquarium*

There were eight linear features that could be extracted from the Shanghai Ocean Aquarium. However, two of them were blocked by the adjacent walls and very few terrestrial point clouds were acquired [see Figs. 8(b) and 10]. Hence, six features were then selected according to the point distribution of the façades in this case study. The location of the features used and their corresponding feature parameters are shown in Fig. 10 and Table 2.

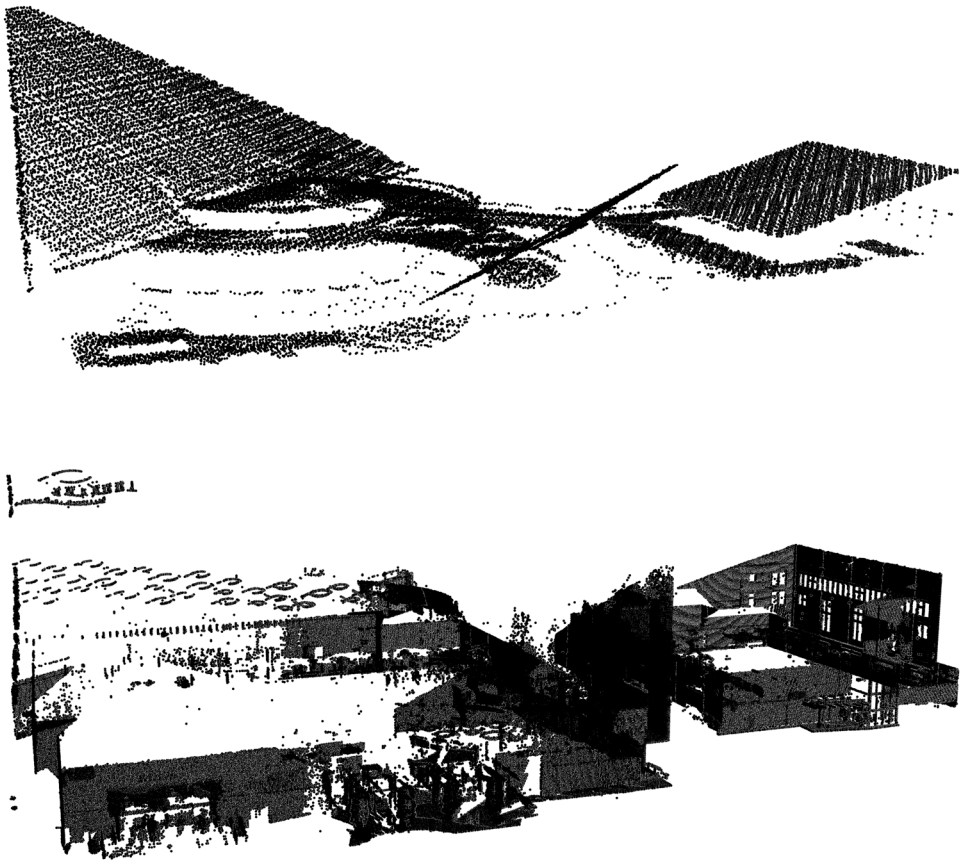

Fig. 8 The second building (Shanghai Ocean Aquarium) used to assess the registration method: (a) ALS point cloud and (b) TLS point cloud.

5.3 *Computation of Parameters*

5.3.1 *Transformation parameters for Pudong ICC*

Using the slope and intercept parameters extracted in Sec. 5.2.1 and the linearized Eqs. (27) and (29) in Appendix A, the adjusted parameters of the simplified similarity transformation model were calculated and are shown in Table 3.

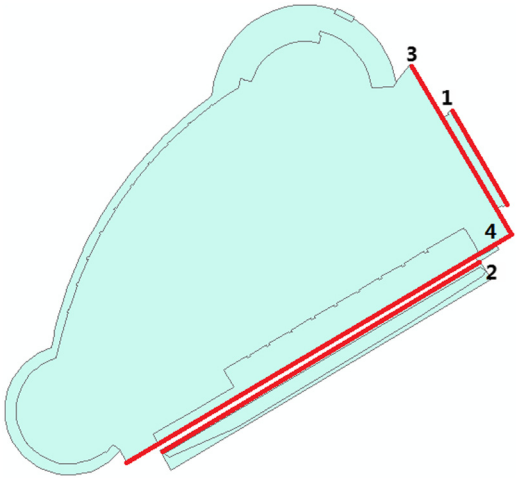

Fig. 9 The linear features extracted from the ALS and TLS datasets of the building adopted as a case study. Numbers in this figure mean the ID of each feature.

Table 1 The slope and intercept parameters of the linear features.

	Parameters of terrestrial line features		Parameters of airborne line features	
ID	*K*	*B*	*K*	*B*
1	1.0768	254.55	−1.6862	4865.53
2	−0.9278	84.73	0.5922	−796.06
3	1.0769	260.40	−1.6831	4866.25
4	−0.9278	84.33	0.5911	−791.97

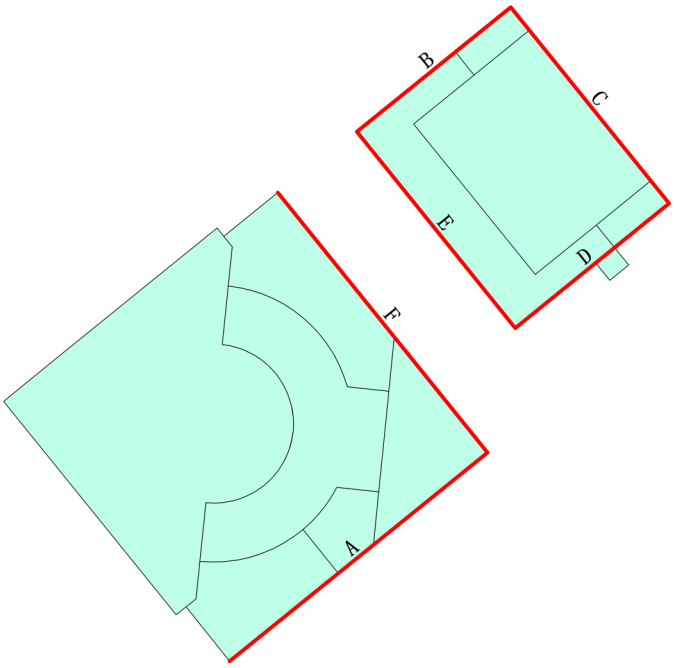

Fig. 10 The linear features extracted from the ALS and TLS datasets on the Shanghai Ocean Aquarium building. Letters in this figure denote the ID of each feature.

Table 2 The slope and intercept parameters of linear features.

	Parameters of terrestrial line features		Parameters of airborne line features	
ID	*K*	*B*	*K*	*B*
A	−3.1912	−18.40	0.8074	−1552.38
B	−3.1194	−234.07	0.8010	−1460.71
C	0.3217	−6.21	−1.2385	4494.07
D	−3.1193	−75.86	0.8471	−1648.73
E	0.3197	−47.01	−1.3040	4430.80
F	0.3219	−64.99	−1.2374	4398.64

Table 3 Results for the model parameters after the adjustment for the Pudong ICC building.

Parameters	Value of the proposed method
α^0	106.6149 ± 0.0248
Δx (m)	2302.56 ± 0.24
Δy (m)	641.01 ± 1.21
Δz (m)	6.79 ± 0.02
μ	1.0074202 ± 0.00030

5.3.2 *Transformation parameters for Shanghai Ocean Aquarium building*

Using the feature parameters listed in Table 2 and the linearized Eqs. (27) and (29), the transformation parameters of the Shanghai Ocean Aquarium building were listed in Table 4.

5.4 *Accuracy Evaluation*

The real accuracy evaluation is important for a coordinate matching case. In this paper, some points of two buildings were selected to implement the real accuracy evaluation processing. Moreover, an overlap area of the Pudong ICC building exists in the eaves, therefore, a real accuracy evaluation was also performed for this part.

5.4.1 *Check point extraction and evaluation of the accuracy for two buildings*

In this experiment, the two kinds of checkpoints of the Pudong ICC building were selected to evaluate the real horizontal and vertical accuracies after registration.

The first type (TYPE-1), contains five points and is the center of the sphere or cylinder. Among them, two were the centers of spheres, and the other three were the centers of cylinders. First, the points belonging to different cylinders and spheres were manually selected. Then, a center-fitting program was applied to measure the corresponding primitives. The original coordinates of the checkpoints in the source (TLS) and target (ALS) reference systems were calculated.

The second type (TYPE-2) is the corner of the building roof and contains six points. The coordinates of the second type of checkpoints were manually selected. Using the parameters of the estimated simplified similarity transformation model, each checkpoint from the TLS point cloud was mapped onto the target ALS system.

A comparison was then conducted to evaluate the difference between the transformed and known coordinates. The results and RMSE of each set of coordinates are shown in Table 5, where ΔP denotes the horizontal positional accuracy

Table 4 Results for the model parameters after the adjustment for the Shanghai Ocean Aquarium building.

Parameters	Value of the proposed method
α^0	249.1204 ± 0.0177
Δx (m)	2965.71 ± 0.29
Δy (m)	828.91 ± 0.88
Δz (m)	4.79 ± 0.02
μ	1.0034707 ± 0.00020

Table 5 Coordinate differences of checkpoints and corresponding root-mean-square error (RMSE) of Pudong ICC building.

Type	Index	ΔX	ΔY	ΔZ	ΔP	$RMSE_{\Delta X}$	$RMSE_{\Delta Y}$	$RMSE_{\Delta Z}$
TYPE-1	S1	0.007	−0.031	−0.235	0.032	0.120	0.085	0.200
	S2	−0.095	0.106	0.248	0.142			
	A1	−0.190	−0.041	−0.241	0.194			
	C1	0.149	0.010	0.147	0.149			
	C2	0.072	−0.149	0.081	0.165			
TYPE-2	J1	0.006	−0.398	0.086	0.398	0.190	0.276	0.243
	J2	−0.190	−0.362	0.107	0.408			
	J3	0.227	0.287	0.335	0.365			
	J4	0.035	0.078	0.392	0.085			
	J5	−0.287	−0.177	−0.222	0.337			
	J6	0.107	0.095	0.128	0.143			

$$\Delta P = \sqrt{\Delta X^2 + \Delta Y^2}. \tag{20}$$

Then, the total transformation accuracy is evaluated by computing the RMSE of each coordinate departure (see Table 5). Compared with the accuracy results of TYPE-1 and TYPE-2 checkpoints, we can find that the accuracy of TYPE-1 checkpoints is greater than TYPE-2. This is because the TYPE-1 checkpoints are obtained by fitting a point cloud, and the accuracy is better than TYPE-2 checkpoints.

Six corner points are also manually selected from the Shanghai Ocean Aquarium building. The total transformation accuracy is evaluated by computing the RMSE of each coordinate departure (see Table 6).

Comparing Table 6 with Table 5, we find that the horizontal accuracy of the two buildings can reach 0.15 to 0.50 m. Also, the vertical accuracy is great than 0.25 m.

5.4.2 *Overlap zone accuracy evaluation for Pudong ICC building*

The eaves of the Pudong ICC (see line 2 part in Fig. 9) were used to evaluate the residuals after registration in the overlap portion between the ALS and TLS datasets. The ALS system collected the point's coordinates of the eaves from the top view, while the TLS system captured the point's

Table 6 Coordinate differences of checkpoints and corresponding RMSE of Shanghai Ocean Aquarium building.

Index	ΔX	ΔY	ΔZ	ΔP	$RMSE_{\Delta X}$	$RMSE_{\Delta Y}$	$RMSE_{\Delta Z}$
Q1	0.200	0.177	0.001	0.267	0.258	0.288	0.201
Q2	−0.279	0.361	0.147	0.456			
Q3	0.293	−0.270	0.354	0.476			
Q4	0.188	−0.294	0.065	0.486			
Q5	0.158	−0.348	−0.139	0.382			
Q6	−0.285	−0.136	0.368	0.408			

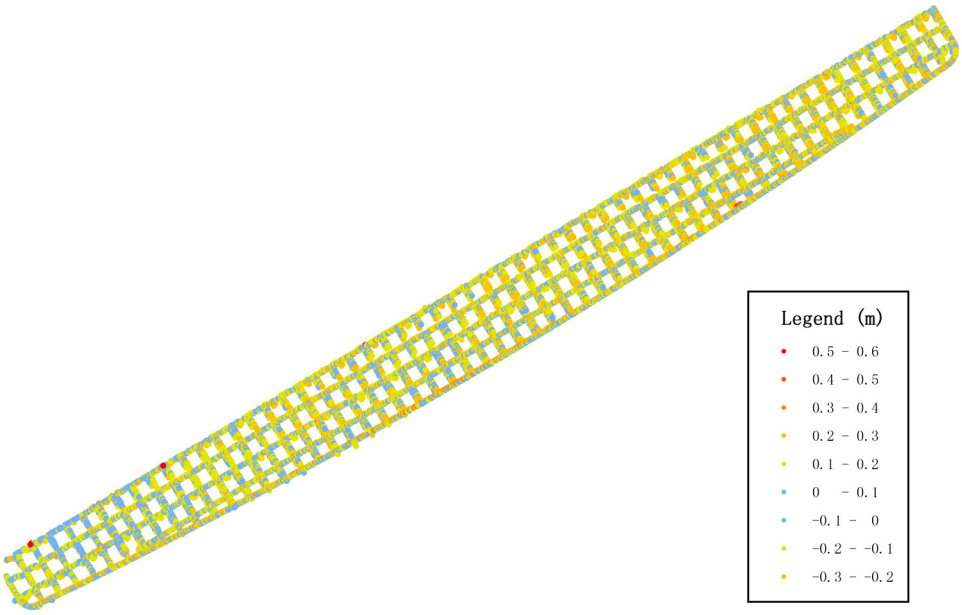

Fig. 11 Residuals on the eaves of the Pudong ICC building between the ALS and TLS point clouds after registration.

coordinates from the bottom view. Two main steps were performed. First, the ALS point cloud was used to fit a plane. Then, the transferred TLS point cloud was projected to the fitted plane to obtain the projection difference. The results are graphically shown in Fig. 11.

To evaluate the distribution of the difference levels, the residual data were sliced into nine classes (shown in the first column of Table 7). The number of points in each class was calculated, and the percentage and the cumulative percentage were also computed. It is clear that 99% of the points were in the range between −0.3 and 0.3 m, which indicates that the calculated model parameters worked to match the TLS and ALS point clouds.

5.5 *Registration Results*

According to the model parameters calculated in Sec. 5.3, the TLS point cloud is mapped onto the ALS system. In Fig. 12, the registration results of the two buildings are shown. The color in Fig. 12 represents the data sources of the point cloud. From these figures, we can conclude that the computed parameters worked well for registering data between the reference systems.

Table 7 Number of points in different layers.

Class (m)	# Points	Percentage (%)	Cumulative percentage (%)
−0.3 to −0.2	2637	19.32	19.32
−0.2 to −0.1	3334	24.42	43.74
−0.1 to 0	2527	18.51	62.25
0 to 0.1	2082	15.25	77.50
0.1 to 0.2	1901	13.93	91.43
0.2 to 0.3	1040	7.62	99.05
0.3 to 0.4	120	0.88	99.93
0.4 to 0.5	2	0.01	99.94
0.5 to 0.6	8	0.06	100.00

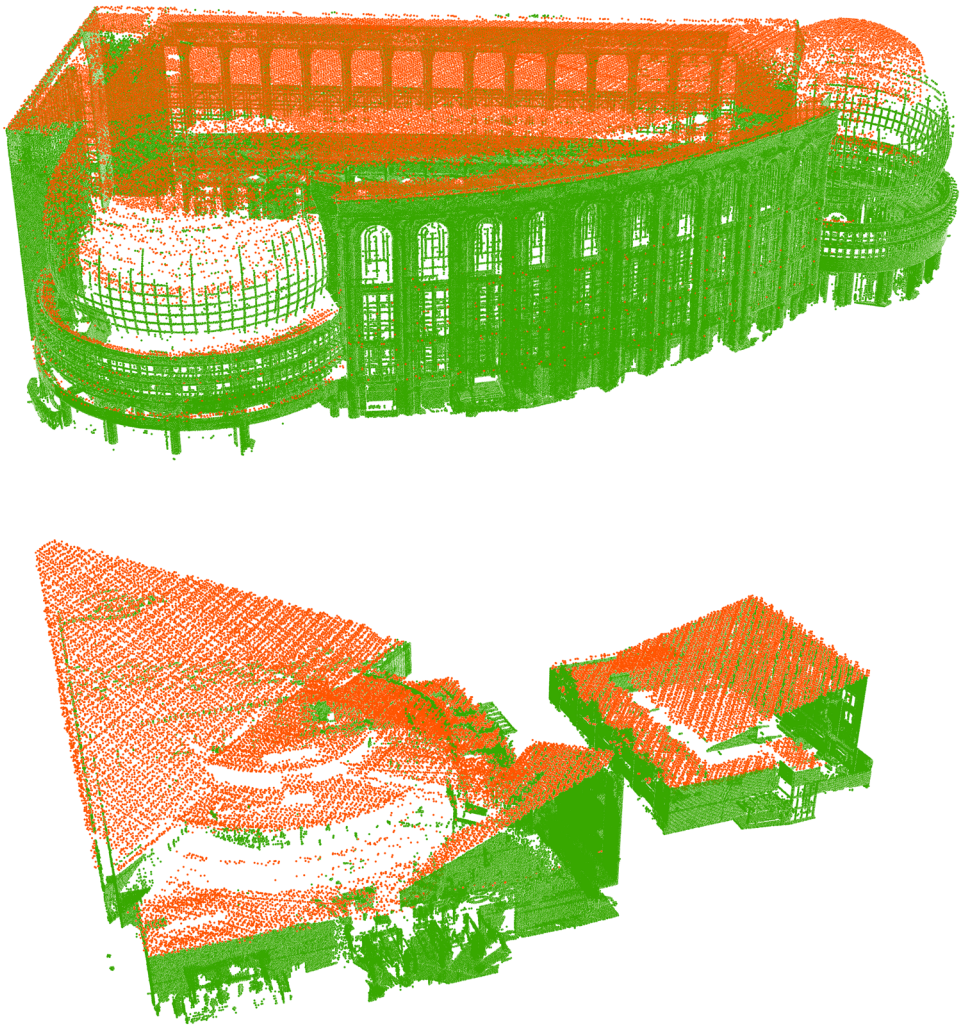

Fig. 12 Visualization of the registration results: (a) Shanghai Pudong ICC and (b) Shanghai Ocean Aquarium.

6 Discussion and Conclusion

With the rapid development of laser scanning technologies, airborne and terrestrial LiDAR data have become important sources for 3-D city modeling and the high-resolution mapping of urban environments. Data fusion of airborne and terrestrial point clouds is likely to be beneficial for the completeness of building modeling because these sensors perform data acquisition from complementary positions. Terrestrial laser scanners usually scan the building façades, while an ALS scans the roof surface. The core issue of the registration method is the 3-D coordinate transformation and parameter calculation. In a more general case, a 3-D similarity transformation model can be adopted to account for differences in scale that might arise, for example, when one dataset is derived from an image-based photogrammetric reconstruction. The manual selection of common points to compute such a transformation is challenging because of the different coverages of the two datasets and the discrete sample modes. This problem is partly overcome here by introducing a new data registration approach based on linear and polygonal features extracted from both the airborne and terrestrial point clouds. The key procedures of this method are as follows: (1) feature extraction and feature parameter calculation in the corresponding reference systems; (2) horizontal model parameter estimation by exploiting linear and polygonal features as constraints after projection onto a horizontal plane; and (3) vertical model parameter computation based on the difference in point height on the building roof between terrestrial and airborne LiDAR data. The experimental results demonstrated that the

proposed method works well for registration between the two types of point clouds. The TLS and ALS point clouds of two buildings were selected to implement the registration. The evaluated accuracy for one of the case studies was ±15 cm in the horizontal direction and ±20 cm in elevation, respectively, in the case of a dataset for which the average distance of the laser scanning point cloud was 12 cm for the terrestrial dataset and 16 cm for the airborne dataset. Further analysis is needed to determine the sensitivity of this procedure to larger point spacing in both point clouds, especially in the airborne dataset, where lower sampling steps at the 50 to 100 cm level are quite common.

The application of the proposed method has some strict requirements. The main condition is that both raw datasets must be referred to as topocentric reference systems, with the vertical Z-axis aligned with the local plumb line. This condition is easy to fulfill in ALS because the data are normally rendered in a topographic reference system. The condition can also be easily achieved with modern terrestrial laser scanners, which are equipped with internal leveling sensors able to compensate for the Z-axis direction. Alternatively, external level plummets or a set of ground control points measured within a geodetic network can provide topocentric coordinates. Of course, this condition may be imperfect in real datasets due to residual errors. When the object lacks a large vertical extension, errors in the vertical alignment of the terrestrial dataset may be neglected. However, they could be significant for high-rise buildings. In this case, the extraction and registration of vertical features between the datasets could help to overcome this problem.

Another requirement of the proposed method involves the roof shape of the building. The precondition for applying this method to compute the horizontal transformation parameters is that the extracted features (both lines and polygons) must be the same objects in the real scene. In the case of an overhanging roof, the feature lines of the ALS point cloud and the feature polygons of the TLS point cloud may be different. In this case, the proposed method could not be used due to the lack of common feature constraints.

The initial values of the model parameters, especially the horizontal parameters, are important for quick convergence to the optimal values. There are two possible solutions. The first is to select some approximate common points and calculate the model parameters by traditional methods, then use the results as initial values. The second solution is based on the use of the feature-constraint functions Eqs. (15) and (16) to calculate the initial value based on two pairs of corresponding features.

The focus of this paper is on the registration procedure, including the model selection and the extraction of common features for its estimate. Further improvements could be based on the use of a wider class of common features to compute the registration parameters.[41]

To incorporate this procedure in an operational pipeline for the fusion of airborne and laser scanning data over large areas, other tasks should be automated, such as the extraction of single buildings from an airborne point cloud. However, these aspects have been widely addressed in the existing literature and have not been dealt with here.[42] In a similar way, the labeling of corresponding features during different steps is manually accomplished now, but the extension toward a fully automatic pipeline is needed for extensive application of this technique.

As already mentioned in Sec. 1, this method could be applied for refining coregistration when terrestrial data have been geo-referenced using a "direct" technique. This case also includes data gathered by a mobile laser scanning system to increase productivity.[43] In particular, this field of application seems highly promising and deserves focused investigation.

Appendix A

Derivation of parameter α from Eq. (15):

$$V_{K_A^{IJ}} = \frac{-\tan\alpha^0 + K_T^{ij}}{1 + K_T^{ij}\tan\alpha^0} + \left(\frac{\partial K_A^{IJ}}{\partial\alpha}\right)_0 \mathrm{d}\alpha - K_A^{IJ}, \tag{21}$$

where α^0 denotes the initial value of parameter α; $\mathrm{d}\alpha$ is the estimated correction of α^0; and $V_{K_A^{IJ}}$ is the correction of observation K_A^{IJ}. The coefficient $[(\partial K_A^{IJ})/(\partial\alpha)]_0$ is given by

$$\left(\frac{\partial K_{\mathrm{A}}^{IJ}}{\partial \alpha}\right)_0 = \frac{K_{\mathrm{T}}^{ij^2}+1}{\rho(\cos\alpha^0 + K_{\mathrm{T}}^{ij}\sin\alpha^0)^2}. \tag{22}$$

Let $l_{K_{\mathrm{A}}^{IJ}}$ be the constant term of Eq. (21)

$$l_{K_{\mathrm{A}}^{IJ}} = K_{\mathrm{A}}^{IJ} - \frac{-\tan\alpha^0 + K_{\mathrm{T}}^{ij}}{1 + K_{\mathrm{T}}^{ij}\tan\alpha^0}. \tag{23}$$

Analogously, Eq. (24) will be converted by total differential to Eq. (16)

$$V_{B_{\mathrm{A}}^{IJ}} = B_{\mathrm{A}}^{IJ^0} + \left(\frac{\partial B_{\mathrm{A}}^{IJ}}{\partial \alpha}\right)_0 \mathrm{d}\alpha + \left(\frac{\partial B_{\mathrm{A}}^{IJ}}{\partial \Delta x}\right)_0 \mathrm{d}\Delta x + \left(\frac{\partial B_{\mathrm{A}}^{IJ}}{\partial \Delta y}\right)_0 \mathrm{d}\Delta y + \left(\frac{\partial B_{\mathrm{A}}^{IJ}}{\partial \mu}\right)_0 \mathrm{d}\mu - B_{\mathrm{A}}^{IJ}, \tag{24}$$

where the coefficients are as follows:

$$\begin{cases} B_{\mathrm{A}}^{IJ^0} = \frac{\mu^0 B_{\mathrm{T}}^{ij} + \Delta y^0(\cos\alpha^0 + K_{\mathrm{T}}^{ij}\sin\alpha^0) + \Delta x^0(\sin\alpha^0 + K_{\mathrm{T}}^{ij}\cos\alpha^0)}{\cos\alpha^0 + K_{\mathrm{T}}^{ij}\sin\alpha^0} \\ \left(\frac{\partial B_{\mathrm{A}}^{IJ}}{\partial \alpha}\right)_0 = \frac{\mu^0 B_{\mathrm{T}}^{ij}(\sin\alpha^0 - B_{\mathrm{T}}^{ij}\cos\alpha^0) + \Delta x^0(1+K_{\mathrm{T}}^{ij^2})}{\rho''(\cos\alpha^0 + K_{\mathrm{T}}^{ij}\sin\alpha^0)^2} \\ \left(\frac{\partial B_{\mathrm{A}}^{IJ}}{\partial \Delta x}\right)_0 = \frac{\sin\alpha^0 - K_{\mathrm{T}}^{ij}\cos\alpha^0}{\cos\alpha^0 + K_{\mathrm{T}}^{ij}\sin\alpha^0} \\ \left(\frac{\partial B_{\mathrm{A}}^{IJ}}{\partial \Delta y}\right)_0 = 1 \\ \left(\frac{\partial B_{\mathrm{A}}^{IJ}}{\partial \mu}\right)_0 = \frac{B_{\mathrm{T}}^{ij}}{\cos\alpha^0 + K_{\mathrm{T}}^{ij}\sin\alpha^0} \end{cases}. \tag{25}$$

Let $l_{B_{\mathrm{A}}^{IJ}}$ be the constant term of Eq. (24)

$$l_{B_{\mathrm{A}}^{IJ}} = B_{\mathrm{A}}^{IJ} - B_{\mathrm{A}}^{IJ^0}. \tag{26}$$

According to the above analysis, the plane parameters of the simplified Bursa model can be calculated by

$$V_{2q\times 1} = \mathrm{A}_{2q\times 4}\widehat{\mathrm{d}\Xi_{\mathrm{h}}} - l_{2q\times 1}, \tag{27}$$

where q denotes the number of line-feature pairs, V denotes the residuals of the observations after the LS estimate (the slope and intercept value of line-feature pairs), and $\widehat{\mathrm{d}\Xi_{\mathrm{h}}}$ denotes the correction to the model parameters Ξ_{h}. The design matrix A is as follows:

$$A = \begin{bmatrix} \frac{K_{\mathrm{T}}^{ij2}+1}{\rho''(\cos\alpha^0 + K_{\mathrm{T}}^{ij}\sin\alpha^0)^2} & 0 & 0 & 0 \\ \frac{\mu^0 B_{\mathrm{T}}^{ij}(\sin\alpha^0 - B_{\mathrm{T}}^{ij}\cos\alpha^0) + \Delta x^0(1+K_{\mathrm{T}}^{ij2})}{\rho''(\cos\alpha^0 + K_{\mathrm{T}}^{ij}\sin\alpha^0)^2} & \frac{\sin\alpha^0 - K_{\mathrm{T}}^{ij}\cos\alpha^0}{\cos\alpha^0 + K_{\mathrm{T}}^{ij}\sin\alpha^0} & 1 & \frac{B_{\mathrm{T}}^{ij}}{\cos\alpha^0 + K_{\mathrm{T}}^{ij}\sin\alpha^0} \\ \cdots & \cdots & \cdots & \cdots \\ \cdots & \cdots & \cdots & \cdots \end{bmatrix}_{2q\times 4}. \tag{28}$$

Vector l includes the constant terms

$$l = \begin{bmatrix} K_{\mathrm{A}}^{IJ} - \frac{-\tan\alpha^0 + K_{\mathrm{T}}^{ij}}{1 + K_{\mathrm{T}}^{ij}\tan\alpha^0} \\ B_{\mathrm{A}}^{IJ} - \frac{\mu^0 B_{\mathrm{T}}^{ij} + \Delta y^0(\cos\alpha^0 + K_{\mathrm{T}}^{ij}\sin\alpha^0) + \Delta x^0(-K_{\mathrm{T}}^{ij}\cos\alpha^0 + \sin\alpha^0)}{\cos\alpha^0 + K_{\mathrm{T}}^{ij}\sin\alpha^0} \\ \cdots \\ \cdots \end{bmatrix}_{2q\times 1}. \tag{29}$$

Acknowledgments

This paper is supported by the National Science Foundation of China (Grants Nos. 41101382 and 41371333), the National High Technology Research and Development Program of China (No. 2013AAA206) and the National Basic Research Program of China (No. 2013CB733204).

The authors thank the Shanghai Surveying and Mapping Institute for supplying the airborne point cloud and also would like to thank the anonymous reviewers for their comments and useful suggestions.

References

1. C. Brenner, "Building reconstruction from images and laser scanning," *Int. J. Appl. Earth Obs. Geoinf.* **6**(3–4), 187–198 (2005).
2. J. Shan and C. K. Toth, *Topographic Laser Scanning and Ranging: Principles and Processing*, pp. 590, Taylor and Francis Group, Boca Raton, Florida (2008).
3. G. Vosselman and H.-G. Maas, *Airborne and Terrestrial Laser Scanning*, pp. 320, Taylor and Francis Group, Boca Raton, Florida (2010).
4. M. Holopainen et al., "The use of ALS, TLS and VLS measurements in mapping and monitoring urban trees," in *Proc. of IEEE Joint Urban Remote Sensing Event (JURSE)*, IEEE, Piscataway (2011).
5. T. Luhmann et al., *Close Range Photogrammetry: 3D Imaging Techniques*, pp. 702, Walter De Gruyter Inc., Berlin, Germany (2013).
6. F. Remondino and J. Böhm, "Editorial of special issue on terrestrial 3D modeling," *ISPRS J. Photogramm. Remote Sens.* **76**(1), 31–32 (2013).
7. D. Novak and K. Schindler, "Approximate registration of point clouds with large scale differences," *ISPRS Ann. Photogramm. Remote Sens. Spatial Inf. Sci.* **Part 5**(W2), 211–216 (2013).
8. P. Theiler and K. Schindler, "Automatic registration of terrestrial laser scanner point clouds using natural planar surfaces," *Int. Ann. Photogramm. Remote Sens. Spatial Inf. Sci.* **39**(Part 3), 86–91 (2012).
9. L. Bornaz, A. Lingua, and F. Rinaudo, "A new software for the automatic registration of 3D digital models acquired using laser scanner devices," in *Proc. of 2002CIPA WG6 Int. Workshop for Cultural Heritage Recording*, Corfu, pp. 52–57, scanning.fh-mainz.de, Mainz, Germany (1–2 September 2002).
10. M. Scaioni, "On the estimation of rigid-body transformation for TLS registration," *Int. Arch. Photogramm. Remote Sens. Spatial Inf. Sci.* **XXXIX-B5**(Part B5), 601–606 (2012).
11. P. Besl and N. McKay, "A method for registration of 3-D shapes," *IEEE Trans. Pattern Anal. Mach. Intell.* **14**(2), 239–256 (1992).
12. Y. Chen and G. Medioni, "Object modelling by registration of multiple range images," *Image Vision Comput.* **10**(3), 145–155 (1992).
13. T. Masuda and N. Yokoya, "A robust method for registration and segmentation of multiple range images," *Comput. Vision Image Understand.* **61**(3), 295–307 (1995).
14. R. Bergevin et al., "Towards a general multi-view registration technique," *IEEE Trans. Pattern Anal. Mach. Intell.* **18**(5), 540–547 (1996).
15. J. Salvi et al., "A review of recent range image registratioon methods with accuracy evaluation," *Image Vision Comput.* **25**(5), 578–596 (2007).
16. L. Cheng et al., "Semi-automatic registration of airborne and terrestrial laser scanning data using building corner matching with boundaries as reliability check," *Remote Sens.* **5**(12), 6260–6283 (2013).
17. L. Zhong et al., "An automatic technique for registering airborne and terrestrial LiDAR data," in *The 21st Int. Conf. on Geoinformatics*, IEEE, Kaifeng, China (2013).
18. D. Lowe, "Distinctive image features from scale-invariant keypoints," *Int. J. Comput. Vision* **60**(2), 91–110 (2004).
19. H. Bay et al., "Speeded-up robust features (SURF)," *Comput. Vision Image Understand.* **110**(3), 346–359 (2008).
20. D. D. Lichti and J. C. K. Chow, "Inner constraints for planar features," *Photogramm. Rec.* **28**(141), 74–85 (2013).
21. A. A. Goshtasby, *2-D and 3-D Image Registration: for Medical, Remote Sensing, and Industrial Applications*, 1st ed., pp. 77–86, Wiley-Interscience, New Jersey (2005).

22. G. Roth, "Registration two overlapping range images," in *IEEE Int. Conf. on 3D Imaging and Modeling*, Ottawa, pp. 191–200, IEEE, Piscataway (4–8 October 1999).
23. J. K. Seo, G. C. Sharp, and S. W. Lee, "Range data registration using photometric features," in *Proc. of IEEE Computer Society Conf. on Computer Vision and Pattern Recognition*, Vol. 2, pp. 1140–1145, IEEE, Piscataway (20–25 June 2005).
24. X. Li and I. Guskov, "Multiscale features for approximate alignment of point-based surfaces," in *Proc. of the Third Eurographics Symposium on Geometry Processing (SGP)*, Vienna, Austria, pp. 217–226, Eurographics Association Aire-la-Ville, Switzerland (4–6 July 2005).
25. M. I. Alba et al., "Automatic registration of multiple laser scans using panoramic RGB and intensity images," *Int. Arch. Photogramm. Remote Sens. Spatial Inf. Sci.* **38**(Part 5W12), 6 (2011).
26. M. Weinmann, S. Hinz, and B. Jutzi, "Fast and automatic image-based registration of TLS data," *ISPRS J. Photogramm. Remote Sens.* **66**(6), S62–S70 (2011).
27. C. Dold and C. Brenner, "Registration of terrestrial laser scanning data using planar patches and image data," *Int. Arch. Photogramm. Remote Sens. Spatial Inf. Sci.* **36**(Part 5), 25–27 (2006).
28. K. Bae and D. Lichti, "A method for automated registration of unorganized point clouds," *ISPRS J. Photogramm. Remote Sens.* **63**(1), 36–54 (2008).
29. F. Crosilla, D. Visintini, and F. Sepic, "Reliable automatic classification and segmentation of laser point clouds by statistical analysis of surface curvature values," *Appl. Geomat.* **1**(1), 17–30 (2009).
30. W. Hansen, H. Gross, and U. Thoennessen, "Line-based registration of terrestrial and aerial LiDAR data," *Int. Arch. Photogramm. Remote Sens. Spatial Inf. Sci.* **37**(B3a), 161–166 (2008).
31. A. H. Mohamed and B. E. Wilkinson, "Direct georeferencing of stationary LiDAR," *Remote Sens.* **1**(4), 1321–1337 (2009).
32. J.-A. Paffenholz, "Direct geo-referencing of 3D point clouds with 3D positioning sensors," Ph.D. Thesis, German Geodetic Commission (DGK), München (2012).
33. D. D. Lichti, S. J. Gordon, and T. Tipdecho, "Error models and propagation in directly georeferenced terrestrial laser scanner networks," *J. Eng. Surv.* **131**(4), 135–142 (2005).
34. M. Scaioni, "Direct georeferencing of TLS in surveying of complex sites," *Int. Arch. Photogramm. Remote Sens. Spatial Inf. Sci.* **36**(Part 5/W17), 8 (2005).
35. P. J. Rousseeuw and A. M. Leroy, *Robust Regression and Outlier Detection*, pp. 329, John Wiley, New York (1987).
36. B. Yang, W. Xu, and Z. Dong, "Automated building outlinesextraction from airborne laser scanning point clouds," *IEEE Geosci. Remote Sens. Lett.* **10**(6), 1399–1403 (2013).
37. J. F. Canny, "A computational approach to edge detection," *IEEE Trans. Pattern Anal. Mach. Intell.* **PAMI-8**(6), 679–698 (1986).
38. B. Yang and Z. Dong, "A shape-based segmentation method for mobile laser scanning point clouds," *ISPRS J. Photogramm. Remote Sens.* **81**, 19–30 (2013).
39. B. Yang and Z. Wei, "Semi-automated building facade footprint extraction from mobile lidar point clouds," *IEEE Geosci. Remote Sens. Lett.* **10**(4), 766–770 (2013).
40. M. Previtali et al., "Automatic façade segmentation for thermal retrofit," *Int. Arch. Photogramm. Remote Sens. Spatial Inf. Sci.* **40**(Part 5/W1), 197–204 (2013).
41. L. Liu and I. Stamos, "A systematic approach for 2D-image to 3D-range registration in urban environments," *Comput. Vision Image Understand.* **116**(1), 25–37 (2012).
42. G. Forlani et al., "Complete classification of raw LIDAR data and 3D reconstruction of buildings," *Pattern Anal. Appl.* **8**(4), 357–374 (2006).
43. D. Barber, J. Mills, and S. Smith-Vorsey, "Geometric validation of a ground-based mobile laser scanning system," *ISPRS J. Photogramm. Remote Sens.* **63**(1), 128–141 (2008).

Hangbin Wu received his PhD degree in geodesy and surveying engineering from Tongji University in 2010. He is a lecturer at Tongji University, China. He is the author of more than 20 journal papers. His current research interests include data processing of terrestrial and airborne laser scanning data, sensor network, and geographical information system.

Marco Scaioni, achieved a PhD in geodetic and mapping sciences at Politecnico di Milano, Italy. He is professor of Tongji University, China. He is chairman of the ISPRS Working Group V/3 on terrestrial 3D imaging and sensors. He is associate editor of *Applied Geomatics* (Springer) and the *European Journal of Remote Sensing*. His main research interests are the application of close-range photogrammetry and laser scanning for deformation monitoring and geo-hazard management.

Chun Liu works as a professor at the Tongji University, China. He worked as a research fellow at The Hong Kong Polytechnic University, Nottingham University and The Ohio State University, respectively. His research interests focus on spatial data quality, LiDAR data processing, and integrated geographical data and GPS measurements for urban and engineering applications. He has near 100 publications covering the geographic information science, integration of 3S and imagery processing.

Biographies of the other authors are not available.